

## NEW BOUNDED SKEW CENTRAL DIFFERENCE SCHEME, PART I: FORMULATION AND TESTING

F. Moukalled & M. Darwish

To cite this article: F. Moukalled & M. Darwish (1997) NEW BOUNDED SKEW CENTRAL DIFFERENCE SCHEME, PART I: FORMULATION AND TESTING, Numerical Heat Transfer, Part B: Fundamentals, 31:1, 91-110, DOI: [10.1080/10407799708915101](https://doi.org/10.1080/10407799708915101)

To link to this article: <http://dx.doi.org/10.1080/10407799708915101>



Published online: 19 Apr 2007.



Submit your article to this journal [↗](#)



Article views: 77



View related articles [↗](#)



Citing articles: 11 View citing articles [↗](#)

## NEW BOUNDED SKEW CENTRAL DIFFERENCE SCHEME, PART I: FORMULATION AND TESTING

*F. Moukalled and M. Darwish*

*American University of Beirut, Faculty of Engineering & Architecture,  
Mechanical Engineering Department, P.O. Box 11-0236, Beirut, Lebanon*

*The skew central difference scheme is combined with the normalized variable formulation to yield a new bounded skew central difference scheme. The newly developed scheme is tested and compared with the upwind scheme, the bounded skew upwind scheme, and the high-resolution SMART scheme by solving four problems: (1) pure convection of a step profile in an oblique velocity field; (2) sudden expansion of an oblique flow field in a rectangular cavity; (3) driven flow in a skew cavity; and (4) gradual expansion in an axisymmetric, nonorthogonal channel. Results generated reveal the new scheme to be bounded and to be the most accurate among those investigated.*

### INTRODUCTION

When solving numerical transfer phenomena problems, one of the main sources of error in calculating the convective flux is numerical diffusion in both the cross-stream and streamwise directions. Cross-stream diffusion occurs in a multidimensional flow [1–3] when gradients in a convected quantity exist perpendicular to the flow and the direction of flow is oblique to the grid lines. Streamwise diffusion takes place when gradients in a convected quantity exist parallel to the flow [4], even in one-dimensional situations. Over the last decade, researchers have tried to suppress this error by either reducing streamwise diffusion through the use of higher-order schemes [5–7] or by decreasing cross-stream diffusion by employing skew upwind schemes [8–11]. Both approaches are more accurate than the highly diffusive first-order upwind scheme, but they suffer from a lack of boundedness; i.e., they tend to give rise to nonphysical oscillations that induce large errors, known as numerical dispersion [12].

To suppress numerical dispersion, a variety of procedures have also been reported. These procedures can be divided into two major categories, known as the flux-blending technique and the flux-limiter approach. Methods based on the blending strategy may also be decomposed into two classes. In the first class, a limiting antidiffusive flux is added to a first-order upwind scheme [13] in such a way that the resulting scheme is capable of resolving sharp gradients without undue under- or overshoots. In the second class, however, an opposite route is followed,

Received 15 April 1996; accepted 3 July 1996.

Financial support provided by the University Research Board of the American University of Beirut through Grants 48120 and 48122 and are gratefully acknowledged.

Address correspondence to Professor Fadl Moukalled, Department of Mechanical Engineering, American University of Beirut, P.O. Box 11-0236, Beirut, Lebanon. E-mail: memouk@aub.edu.lb

### NOMENCLATURE

$a$	coefficient in finite-difference equation	$\alpha, \beta, \gamma$	metric quantities
$b$	source term in the discretized equation	$\Gamma$	diffusion coefficient
$B$	volume integral of $Q$	$\eta$	transformed coordinate
$C$	convective flux coefficient	$\nu$	kinematic viscosity
$e$	east face of a control volume	$\xi$	transformed coordinate
$E$	east neighbor of the $P$ grid point	$\rho$	density
$f(\ )$	functional relationship	$\phi$	dependent variable
$G_1, G_2$	convective terms normal to grid cell boundaries		
$J$	Jacobian; total scalar flux across cell face	<b>Subscripts</b>	
$n$	north face of a control volume	$C, D$	central and downstream grid points
$N$	north neighbor of the $P$ grid point	dc	deferred correction
$p$	thermodynamic pressure	$E$	refers to east grid point
$P$	dimensionless pressure; main grid point	$e$	refers to east control-volume face
$Q$	source term in the transport equation	$f$	refers to any of the control-volume faces
$s$	south face of a control volume	$N$	refers to north grid point
$S$	south neighbor of the $P$ grid point	nb	refers to neighbors
$u, U$	dimensional and dimensionless $x$ velocities	$P$	refers to main grid point
$u, V$	dimensional and dimensionless $y$ velocities	$S$	refers to south grid point
$w$	west face of a control volume	$U$	upstream grid point
$W$	west neighbor of the $P$ grid point	$W$	refers to West grid point
$x, X$	dimensional and dimensionless coordinates along the horizontal direction	<b>Superscripts</b>	
$y, Y$	dimensional and dimensionless coordinates along the vertical direction	-	refers to normalized variable
		$C$	convection contribution
		$D$	diffusion contribution
		$U$	upwind formulation

where, starting with an unbounded higher-order scheme, some kind of smoothing diffusive agency is introduced into the scheme so as to damp oscillations [14–16]. In general, because of their multistep nature and the difficulty in balancing the two fluxes, accurate flux-blending techniques tend to be very expensive computationally. A cheaper way to remove nonphysical oscillation is to use the flux-limiter approach. This technique is based on modifying the numerical flux at the interface of the computational cell by the use of a flux limiter that enforces a monotonicity (boundedness) criterion. Higher-order schemes bounded by this approach are usually denoted by high-resolution schemes. The family of “shock-capturing” schemes based on the total variational diminishing flux limiters (TVD) [17], widely used in compressible flow simulations, are well-known examples of this technique. A more recent formulation for high-resolution flux limiters has been developed by Leonard based on the normalized variable formulation (NVF) [18].

A literature survey reveals that most unbounded higher-order schemes have been bounded through the use of one or more of the above methods [18–21]. On the other hand, only a few workers have implemented bounded streamline schemes. The unbounded skew upwind difference and the skew upwind weighted-difference

schemes were initially developed by Raithby [9]. Sharif and Busnaina [22] bounded the skew upwind difference scheme (SUDS) and the second-order upwind difference scheme (SOU DS) using the flux-corrected transport (FCT) method developed by Boris and Book [23] and the filtering remedy and methodology (FRAM) proposed by Chapman [14]. Sharif [11] have also used the FCT method to bound the directional transportive upwind differencing scheme (DTUDS). These bounding techniques follow the flux-blending approach and are thus expensive. More recently, Darwish and Moukalled [24] advertised a new approach to bound skew schemes and applied it to the skew upwind scheme. The resulting NVF SUDS [24] was applied to purely convective problems in Cartesian coordinates, and its performance was found to be impressive. However, for problems in which the variations in the source term are important, as in buoyancy-driven and suddenly expanding flows, the performance of the first-order skew upwind scheme degrades [3]. This degradation in performance is due to the importance of streamwise diffusion, which cannot be resolved by a first-order interpolation profile. To reduce both components of diffusion, a streamline-based scheme of higher order should be used.

To this end, a similar approach to that in [24] is adopted in this work to bound the skew central difference scheme. This is done by combining the skew central difference scheme (SCDS) with the NVF bounding approach to yield a composite skew high-resolution scheme (NVF SCDS) with a light increase in computational cost in comparison with the unbounded SCDS. By going into a higher-order skew scheme, both streamwise and cross-stream diffusion are reduced. Therefore, the resultant scheme should be capable of accurately resolving source-dominated flow problems. Moreover, the applicability of the new approach is extended to flow problems in general planar and axisymmetric curvilinear coordinates. Furthermore, the performance of the newly developed scheme is tested and compared with the upwind scheme, the NVF SUDS, and the high-resolution SMART scheme by solving four problems: (1) pure convection of a step profile in an oblique velocity field; (2) sudden expansion of an oblique flow field in a rectangular cavity; (3) driven flow in a skew cavity; and (4) gradual expansion in an axisymmetric, nonorthogonal channel. Results generated reveal the new scheme to be bounded and to be the most accurate.

## NUMERICAL DISCRETIZATION OF THE TRANSPORT EQUATIONS

The conservation equations governing two-dimensional, incompressible steady-flow problems may be expressed in the following general form:

$$\frac{\partial}{\partial X} \left( \rho U \phi - \Gamma \frac{\partial \phi}{\partial X} \right) + \frac{\partial}{\partial Y} \left( \rho V \phi - \Gamma \frac{\partial \phi}{\partial Y} \right) = Q \quad (1)$$

where  $\phi$  is any dependent variable;  $U$  and  $V$  are the  $X$  and  $Y$  components of the velocity vector;  $\rho$  is the density; and  $\Gamma$  and  $Q$ , specific to a particular meaning of  $\phi$ , are the diffusivity and source term, respectively. Since the new scheme is tested in nonconventional geometry, a general curvilinear boundary-fitted coordinate

system is used. In this coordinate system, Eq. (1) is given by

$$\frac{\partial}{\partial \xi} \left[ \rho G_1 \phi - \frac{\Gamma}{J} \left( \alpha \frac{\partial \phi}{\partial \xi} - \beta \frac{\partial \phi}{\partial \eta} \right) \right] + \frac{\partial}{\partial \eta} \left[ \rho G_2 \phi - \frac{\Gamma}{J} \left( \gamma \frac{\partial \phi}{\partial \eta} - \beta \frac{\partial \phi}{\partial \xi} \right) \right] = QJ \quad (2)$$

where

$$\alpha = \left( \frac{\partial X}{\partial \eta} \right)^2 + \left( \frac{\partial Y}{\partial \eta} \right)^2 \quad \beta = \left( \frac{\partial X}{\partial \xi} \right) \left( \frac{\partial X}{\partial \eta} \right) + \left( \frac{\partial Y}{\partial \xi} \right) \left( \frac{\partial Y}{\partial \eta} \right) \\ \gamma = \left( \frac{\partial X}{\partial \xi} \right)^2 + \left( \frac{\partial Y}{\partial \xi} \right)^2 \quad (3)$$

$$G_1 = U \frac{\partial Y}{\partial \eta} - V \frac{\partial X}{\partial \eta} \quad G_2 = V \frac{\partial X}{\partial \xi} - U \frac{\partial Y}{\partial \xi} \quad J = \frac{\partial X}{\partial \xi} \frac{\partial Y}{\partial \eta} - \frac{\partial X}{\partial \eta} \frac{\partial Y}{\partial \xi} \quad (4)$$

Integrating the above equation over the control volume shown in Figure 1a and applying the divergence theorem, the following discretized equation is obtained:

$$J_e - J_w + J_n - J_s = B \quad (5)$$

where  $J_f$  represents the total flux of  $\phi$  across cell face  $f$  ( $f = e, w, n, \text{ or } s$ ), and  $B$  is the volume integral of the source term  $Q$ . Each of the surface fluxes  $J_f$  contains a convective contribution,  $J_f^C$ , and a diffusive contribution,  $J_f^D$ , hence

$$J_f = J_f^C + J_f^D \quad (6)$$

Along the east face of a control volume, these fluxes are given by

$$J_e^D = - \left( \frac{\Gamma}{J} \right)_e \left( \alpha \frac{\partial \phi}{\partial \xi} - \beta \frac{\partial \phi}{\partial \eta} \right)_e \quad (7)$$

$$J_e^C = (\rho G_1)_e \phi_e \quad (8)$$

The diffusive flux is discretized using a second-order central difference scheme. Along the east face, the discretized form of the diffusive flux is

$$J_e^D = \left( \frac{\Gamma \alpha}{J} \right)_e (\phi_P - \phi_E) + \left( \frac{\Gamma \beta}{J} \right)_e \frac{\phi_{NE} - \phi_{SE} + \phi_N - \phi_S}{4} \quad (9)$$

The fluxes along the west, north, and south faces are found in a similar manner.

The convective flux across face  $f$  can be written as

$$J_f^C = C_f \phi_f \quad (10)$$

where  $C_f$  is the convective flux coefficient at cell face  $f$  ( $\rho G_{1 \text{ or } 2}$ ). As can be seen from Eq. (10), the accuracy of the control-volume solution for the convective scalar flux depends on the proper estimation of the face value  $\phi_f$  as a function of the neighboring  $\phi$  nodes values. Using some assumed interpolation profile,  $\phi_f$  can be explicitly formulated in terms of its node values by a functional relationship of the form

$$\phi_f = f(\phi_{nb}) \quad (11)$$

where  $\phi_{nb}$  denotes the neighboring node  $\phi$  values ( $\phi_E, \phi_W, \phi_N, \phi_S, \phi_{NE}, \phi_{NW}, \phi_{SE}, \phi_{SW}, \dots$ ). After substituting Eq. (11) into Eq. (10) for each cell face and using the resulting equation along with Eq. (9), Eq. (5) is transformed after some algebraic manipulations into the following discretized equation:

$$a_P \phi_P = \sum_{nb} (a_{nb} \phi_{nb}) + b_P \quad (12)$$

where the coefficients  $a_P$  and  $a_{nb}$  depend on the selected scheme and  $b_P$  is the source term of the discretized equation.

Since the functional relationship can involve a large number of neighboring grid points, especially when using higher-order or streamline-based schemes, the solution of Eq. (12) can become very expensive computationally, hence the use of a compacting procedure is most welcome. In the present work the deferred correction procedure of Rubin and Khosla [25] is used. In this procedure, Eq. (5) is rewritten as

$$\begin{aligned} J_e^U - J_w^U + J_n^U - J_s^U \\ = B + \underline{[C_e(\phi_e^U - \phi_e) - C_w(\phi_w^U - \phi_w) + C_n(\phi_n^U \phi_n) - C_s(\phi_s^U - \phi_s)]} \end{aligned} \quad (13)$$

where  $\phi_f^U$  is the face value,  $J_f^U$  is the total flux of  $\phi$ , both calculated using the first-order upwind scheme;  $\phi_f$  is the cell face value calculated using the chosen streamline-based or high-resolution scheme; and the underlined terms represent the extra source term due to the deferred correction. Substituting the value of the cell flux obtained from the functional relationship of the upwind and streamline-based or high-resolution scheme at hand, the deferred correction results in an equation similar in form to Eq. (12), but where the coefficient matrix is pentadiagonal (for two dimensions) and always diagonally dominant, since it is formed using the first-order upwind scheme. The discretized equation, Eq. (12), becomes

$$a_P \phi_P = \sum_{nb} (a_{nb} \phi_{nb}) + b_P + b_{dc} \quad (14)$$

where now the coefficients  $a_p$  and  $a_{nb}$  are obtained from a first-order upwind discretization,  $nb = (E, W, S, N)$ , and  $b_{dc}$  is the extra deferred correction source term. This compacting procedure is simple to implement and very effective when using streamline-based or high-resolution schemes.

### SKEW CENTRAL DIFFERENCE SCHEME

In the skew central difference scheme, the advected values of  $\phi$  at the control-volume faces are approximated by considering the direction of the velocity vector at the cell face and interpolating between the values at the four appropriate nodes among the nodes surrounding the cell face. The two appropriate upstream/downstream nodes are selected by going upstream/downstream along the direction of the velocity vector at the cell face all the way to the line joining the centers of the adjacent cells as shown in Figure 1a. The local profile for  $\phi_c$ , for example, may be obtained as follows:

$$\phi_c = m_1\phi_P + m_2\phi_S + m_3\phi_E + m_4\phi_{NE} \quad (15)$$

where  $m_1$ ,  $m_2$ ,  $m_3$ , and  $m_4$  are weighing factors for  $\phi_P$ ,  $\phi_S$ ,  $\phi_E$ , and  $\phi_{NE}$ , respectively, and depend on the stream direction and the grid. For the configuration shown in Figure 1a, these weighing factors are given by

$$\left\{ \begin{array}{l} m_1 = \frac{d_6}{d_5 + d_6} \frac{d_2}{d_1 + d_2} \\ m_2 = \frac{d_6}{d_5 + d_6} \frac{d_1}{d_1 + d_2} \\ m_3 = \frac{d_5}{d_5 + d_6} \frac{d_3}{d_3 + d_4} \\ m_4 = \frac{d_5}{d_5 + d_6} \frac{d_4}{d_3 + d_4} \end{array} \right. \quad (16)$$

where  $d_1$ ,  $d_2$ ,  $d_3$ ,  $d_4$ ,  $d_5$ , and  $d_6$  are distances defined in Figure 1a.

### NORMALIZED VARIABLE FORMULATION

#### Normalized Variable

The proposed scheme is bounded on the basis of the normalized variable formulation proposed by Leonard [18]. Considering the control volume shown in Figure 1b, defining  $\phi_U$ ,  $\phi_D$ , and  $\phi_C$  as the upstream (U), downstream (D), and central (C) nodal values, the normalized value of  $\phi$  is defined as

$$\bar{\phi} = \frac{\phi - \phi_U}{\phi_D - \phi_U} \quad (17)$$

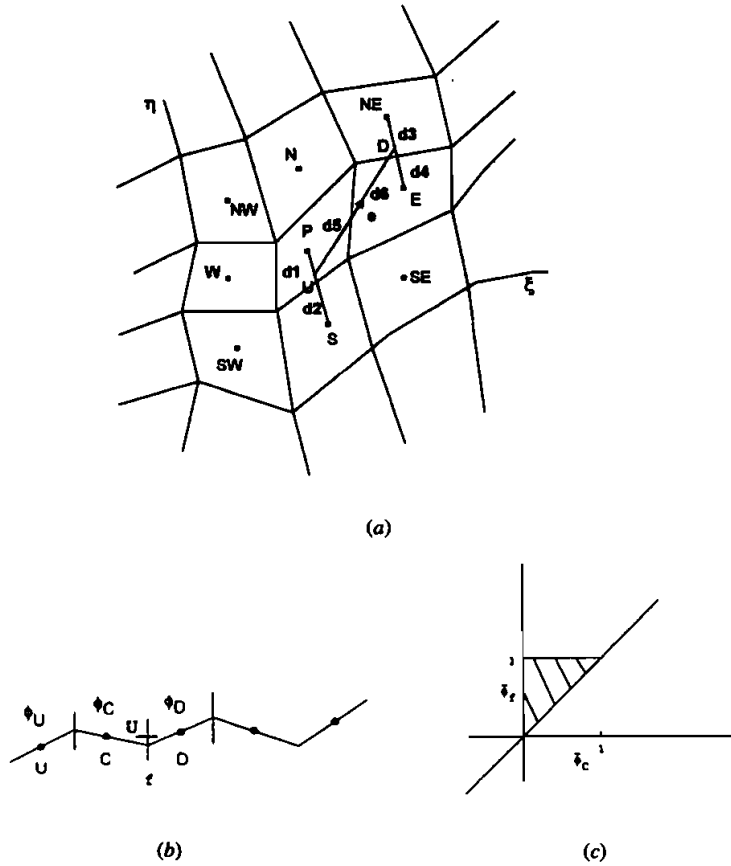


**Figure 1.** (a) Typical grid point cluster, control volume, and SCDS interpolation. (b) Interpolation points used in calculating  $\phi_f$ . (c) Convective boundedness criterion on a normalized variable diagram (NVD).

Note that with this normalization  $\bar{\phi}_D = 1$  and  $\bar{\phi}_U = 0$ . The normalized value of  $\phi$  at a control-volume face is denoted by  $\bar{\phi}_f$ . The use of the normalized variable simplifies the definition of the functional relationships of high-resolution schemes and is helpful in defining the conditions that the functional relationships should satisfy in order to be bounded and numerically stable.

### Convective Boundedness Criterion

Based on the normalized variable analysis, Gaskell and Lau [26] formulated a convection boundedness criterion (CBC) for implicit steady-flow calculation, which states that for a scheme to have the boundedness property, its functional relationship should be continuous, should be bounded from below by  $\bar{\phi}_f = \bar{\phi}_C$ , and from

above by unity, and should pass through the points (0,0) and (1,1), in the monotonic range ( $0 < \tilde{\phi}_C < 1$ ), and for  $1 < \tilde{\phi}_C$  or  $\tilde{\phi}_C < 0$ , the functional relationship  $f(\tilde{\phi}_C)$  should equal  $\tilde{\phi}_C$ . The above conditions, illustrated on a normalized variable diagram (NVD) in Figure 1c, can be formulated as

$$\begin{cases} f(\tilde{\phi}_C) & \text{is continuous} \\ f(\tilde{\phi}_C) = 0 & \text{for } \tilde{\phi}_C = 0 \\ f(\tilde{\phi}_C) = 1 & \text{for } \tilde{\phi}_C = 1 \\ f(\tilde{\phi}_C) < 1 \text{ and } f(\tilde{\phi}_C) > \tilde{\phi}_C & \text{for } 0 < \tilde{\phi}_C < 1 \\ f(\tilde{\phi}_C) = \tilde{\phi}_C & \text{for } \tilde{\phi}_C < 0 \text{ or } \tilde{\phi}_C > 1 \end{cases} \quad (18)$$

### NVF SKEW CENTRAL DIFFERENCE SCHEME

After the calculation of  $\phi_f$  using the skew central difference scheme, the cell face value is normalized to yield  $\tilde{\phi}_f$  and the CBC is enforced in the event when it is not satisfied. It is clear that this modification to the original skew central difference scheme is not difficult to implement and is not expensive computationally.

### CALCULATION OF THE VELOCITY FIELD

So far, the velocity field has been assumed to be known and the methodology to solve for a scalar variable has been presented. For some of the problems considered here, the flow field is unknown. Therefore, to obtain the solution, the continuity and momentum equations should be solved simultaneously. These equations are usually solved on a staggered grid to eliminate the possibility of predicting checkerboard pressure and velocity fields. The use of a staggered grid arrangement with a nonorthogonal curvilinear grid complicates the programming and implementation of the solution algorithm and results in geometric, and related mathematical, complexities. It is therefore desirable, in curvilinear coordinates, to calculate the pressure and velocity components at the same location. However, a special procedure is needed to eliminate the possibility of predicting unrealistic fields. A nonstaggered grid is used in this work, and unrealistic fields are eliminated through the use of the pressure-weighted interpolation method of Peric [15]. Moreover, since the pressure is implicitly specified by the continuity constraint, a pressure correction equation is derived by combining the momentum and continuity equations as in the SIMPLE algorithm [2]. The resulting pressure correction equation in a two-dimensional nonorthogonal coordinate has a computational stencil involving five grid points in each coordinate direction and is very expensive to solve. This has led workers to neglect the nonorthogonal terms to reduce the computational stencil to involve three grid points in each coordinate direction. However, when the grid is highly skewed, Peric [27] reported that the simplified

pressure correction equation does not converge at all or the convergence rate is too slow. In addition, the range of relaxation factors was seen to become narrower for the higher skewness of the nonorthogonal grid. In order not to face these problems, neither here nor in a companion article [28] in which the newly developed scheme is used to solve a natural-convection problem over a highly skew grid, the treatment method for the nonorthogonal terms suggested by Cho and Chung [29] is adopted.

## RESULTS AND DISCUSSION

To check the performance of the new scheme against the upwind, NVF SUDS, and SMART schemes, one purely convective problem and three flow problems are solved. Results are obtained by covering the physical domains with uniform grids. Grid networks are generated using the transfinite interpolation technique [30]. In all tests, computational results are considered converged when the residual error (RE), defined as

$$RE = \text{MAX}_{i=1}^n \left[ \left| a_P \phi_P - \left( \sum_{\text{NB}=\text{E, W, N, S, EE, WW, NN, SS}} a_{\text{NB}} \phi_{\text{NB}} + b_P + b_{dc} \right) \right| \right] \quad (19)$$

becomes smaller than  $10^{-7}$ .

### Test 1: Pure Convection of a Step Profile in an Oblique Velocity Field

Figure 2a shows the well-known benchmark test problem consisting of pure convection of a transverse step profile imposed at the inflow boundaries of a square computational domain. A  $27 \times 27$  mesh is used giving  $\Delta x = \Delta y = 1/25$ . The angle  $\theta$  is chosen to be  $45^\circ$ , and  $|\mathbf{V}| = 1$ . The governing conservation equation of the problem is

$$\frac{\partial(U\phi)}{\partial X} + \frac{\partial(V\phi)}{\partial Y} = 0 \quad (20)$$

where  $\phi$  is the dependent variable and  $U$  and  $V$  are the Cartesian components of the uniform velocity vector  $\mathbf{V}$ . The computed values of  $\phi$  using upwind, SMART, NVF SUDS, NVF SCDS, and the exact analytical solution to the problem are shown, along the vertical centerline of the domain, in Figure 2b. The results presented are very clear and self-explanatory. The best results obtained are for the NVF SCDS and NVF SUDS, which are very smooth, very accurate, and oscillation-free because the CBC criterion is enforced. NVF SCDS performs marginally better than NVF SUDS in this problem, because  $\phi$  is constant in the streamline direction. The results generated by the upwind scheme are highly

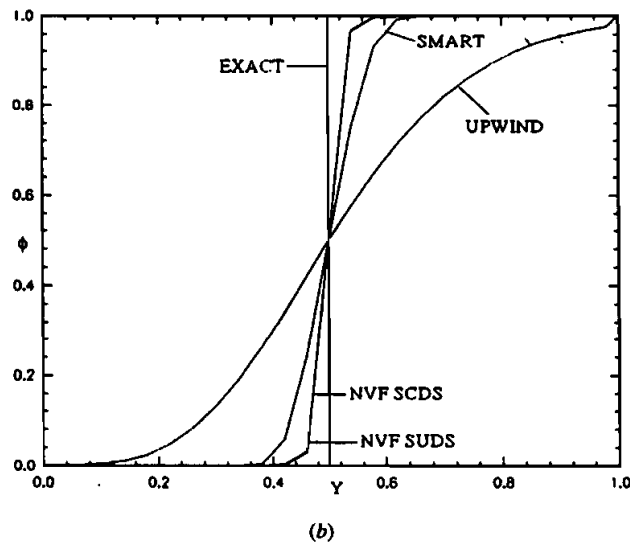
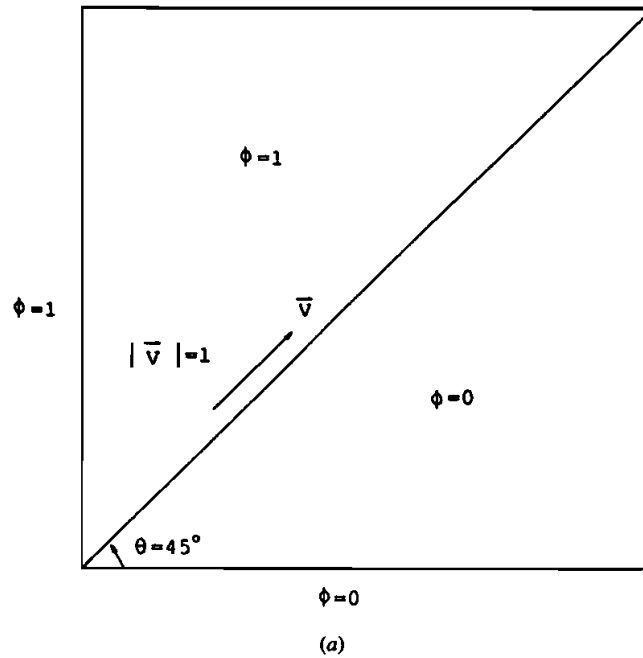


**Figure 2.** (a) Physical domain for pure convection of a scalar discontinuity. (b)  $\phi$  values along the vertical centerline of the domain.

diffusive, as revealed by the smeared profile. The SMART scheme results are much better than those generated by the upwind scheme but of a quality lower than those obtained with the skew schemes, because of the high importance of cross-stream diffusion. The SCDS solution, not presented, did not converge and showed oscillations. These oscillations are the result of the SCDS not satisfying the CBC.

### Test 2: Sudden Expansion of an Oblique Flow Field in a Rectangular Cavity

The physical situation under consideration is depicted in Figure 3a. The flow is assumed to be steady, laminar, and two-dimensional. The nondimensional mass and momentum equations governing the flow field are

$$\frac{\partial U}{\partial X} + \frac{\partial V}{\partial Y} = 0 \quad (21)$$

$$U \frac{\partial U}{\partial X} + V \frac{\partial U}{\partial Y} = -\frac{\partial P}{\partial X} + \frac{1}{\text{Re}} \left( \frac{\partial^2 U}{\partial X^2} + \frac{\partial^2 U}{\partial Y^2} \right) \quad (22)$$

$$U \frac{\partial V}{\partial X} + V \frac{\partial V}{\partial Y} = -\frac{\partial P}{\partial Y} + \frac{1}{\text{Re}} \left( \frac{\partial^2 V}{\partial X^2} + \frac{\partial^2 V}{\partial Y^2} \right) \quad (23)$$

where the following dimensionless variables have been defined:

$$X = \frac{x}{L} \quad Y = \frac{y}{L} \quad U = \frac{u}{V_{\text{ref}}} \quad V = \frac{v}{V_{\text{ref}}} \quad P = \frac{p}{\rho V_{\text{ref}}^2} \quad (24)$$

The boundary conditions used are

$$U = 1 \quad V = 1 \quad \text{at the inlet} \quad (25)$$

$$\frac{\partial U}{\partial X} = \frac{\partial V}{\partial X} = 0 \quad \text{at the exit} \quad (26)$$

$$U = V = 0 \quad \text{elsewhere} \quad (27)$$

The problem is solved using the various schemes for a value of Reynolds number ( $\text{Re} = \rho V_{\text{ref}} L / \mu$ ,  $L$  the cavity height or width and  $V_{\text{ref}}$  the reference velocity) of 400. The  $U$ - and  $V$ -velocity components along the vertical and horizontal centerlines of the domain are presented in Figures 3b and 4a, respectively. In these figures, the profiles obtained using the SMART scheme with a dense grid of size  $42 \times 42$  are compared against the respective profiles generated by the SMART scheme, upwind scheme, NVF SUDS, and NVF SCDS employing  $22 \times 22$  grid points and the upwind scheme using a  $62 \times 62$  grid network. The results in both figures are similar and show the NVF SCDS solution on a coarse grid ( $22 \times 22$ ) to agree very well with the fine-grid SMART solution. The performance of the upwind scheme is very bad, even with the very dense grid. Therefore, for problems in which the flow is highly skew with respect to the grid lines, the upwind scheme should not be used if the size of the grid is to remain reasonable. Because of the importance of cross-stream diffusion, the SMART scheme (a third-order interpolation profile) with  $22 \times 22$  grid points cannot compete with the skew schemes (first-

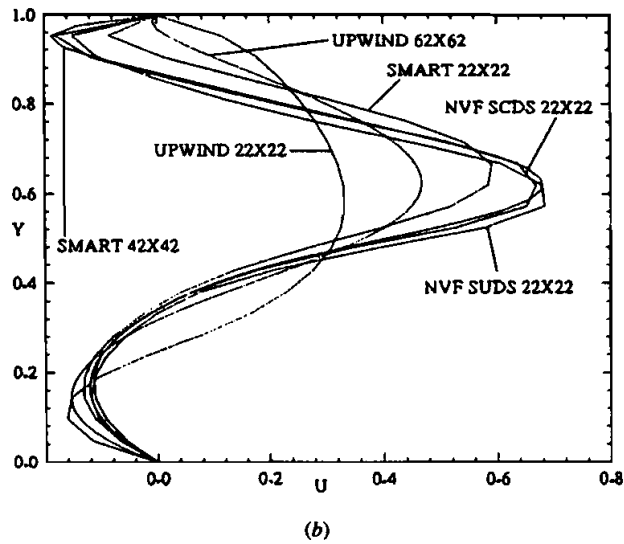
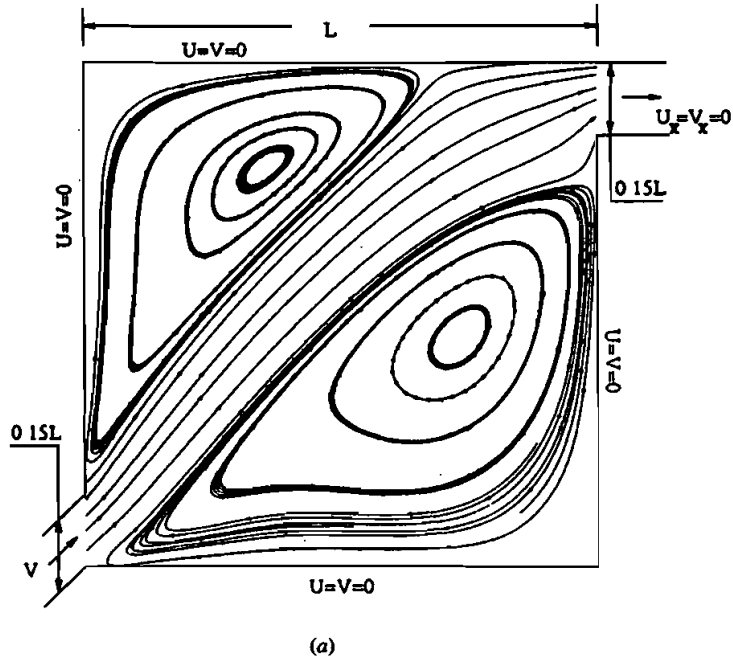


Figure 3. (a) Physical domain, streamlines, boundary conditions, and dimensions for the sudden expansion of an oblique flow field in a rectangular cavity ( $Re = 400$ ). (b)  $U$ -velocity profiles along the vertical centerline of the domain using various schemes.

and second-order interpolation profiles). The NVF SCDS results are better than those generated by the NVF SUDS, but the difference is not very large because of the importance, as mentioned above, of cross-stream diffusion, which is easily resolved by both skew schemes. In Figure 4b, the solutions generated by SMART

using dense grids of sizes  $42 \times 42$  and  $62 \times 62$  are compared against the NVF SCDS results generated on a  $42 \times 42$  grid. This comparison is made in order to test the grid dependency of the NVF SCDS solution. Again, the results generated by the new skew scheme are better than those generated by SMART using a much denser grid. Moreover, it is easily seen that the profile predicted with the SMART scheme on the denser grid approaches the one predicted by NVF SCDS and is expected to fall on top of it if the grid size is increased further.

This problem has clearly demonstrated the importance of resolving cross-stream diffusion and has shown that first- or second-order skew interpolation profiles are by far better than a third-order interpolation profile when the flow field is skew with respect to the grid lines. The next problem will show the virtues of NVF SCDS over NVF SUDS.

### Test 3: Driven Flow in a Skew Cavity

A schematic of the physical situation is given in Figure 5. The governing equations of the problem are the same as for the previous one [Eqs. (21)–(23)]. However, the dimensionless parameters are defined as

$$X = \frac{x}{L} \quad Y = \frac{y}{L} \quad U = \frac{u}{u_s} \quad V = \frac{v}{u_s} \quad P = \frac{p}{\rho u_s^2} \quad (28)$$

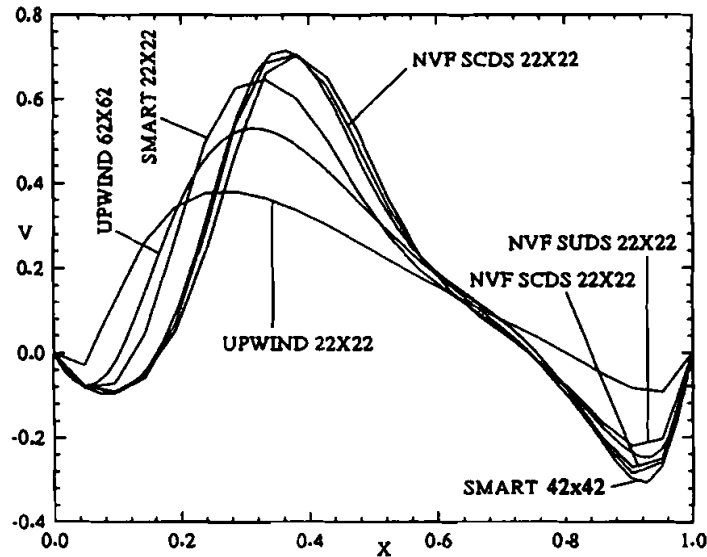
and the applicable boundary conditions are

$$U = 1 \quad V = 0 \quad \text{at } Y = 1 \quad (29)$$

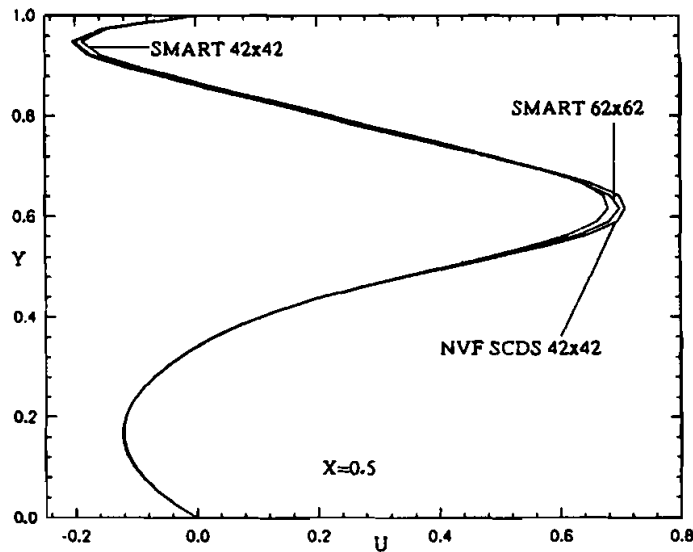
$$U = V = 0 \quad \text{elsewhere} \quad (30)$$

Results are presented for two values of Reynolds number ( $Re = \rho u_s L / \mu$ ,  $L$  the cavity height or width and  $u_s$  the velocity of the top horizontal wall) of 100 and 500. The side walls are skewed at an angle of  $45^\circ$ . The problem is solved using the various schemes and a number of grid sizes. The streamlines for  $Re = 100$  and 500 are depicted in Figures 5a and 5b, respectively. In Figure 5c the results obtained with NVF SCDS and NVF SUDS using a mesh consisting of  $22 \times 22$  grid points are compared, for  $Re = 500$ , against the most accurate results generated by SMART employing a  $62 \times 62$  grid network. (Results obtained with  $42 \times 42$  grid points are as accurate as those generated with the  $62 \times 62$  grid, but the latter are included in order to eliminate any doubts about accuracy.) As shown, the  $U$  profile at  $X = 0.85$  computed by NVF SCDS is very close to the one predicted by SMART. The NVF SUDS profile, however, is of much lower quality and justifies the need to go to streamline-based schemes of higher order when solving problems in which variations in the source term are important.

Comparison of the  $U$ -velocity profile at  $X = 0.85$  generated by NVF SCDS against profiles predicted by SMART and the upwind scheme are depicted in



(a)



(b)

Figure 4. (a)  $V$ -velocity profiles along the horizontal centerline of the domain using various schemes; (b)  $U$ -velocity profiles along the vertical centerline of the domain using dense grids (test 2,  $Re = 400$ ).

Figures 6a and 6b for  $Re = 100$  and  $Re = 500$ , respectively. At  $Re = 100$  (Figure 6a), the profiles are very close, with the one obtained by the NVF SCDS being the closest to that obtained using a denser grid. On the other hand, the profiles for  $Re = 500$  (Figure 6b) are very different and show the NVF SCDS solution on a coarse grid ( $22 \times 22$ ) agreeing very well with the fine-grid SMART solution. The

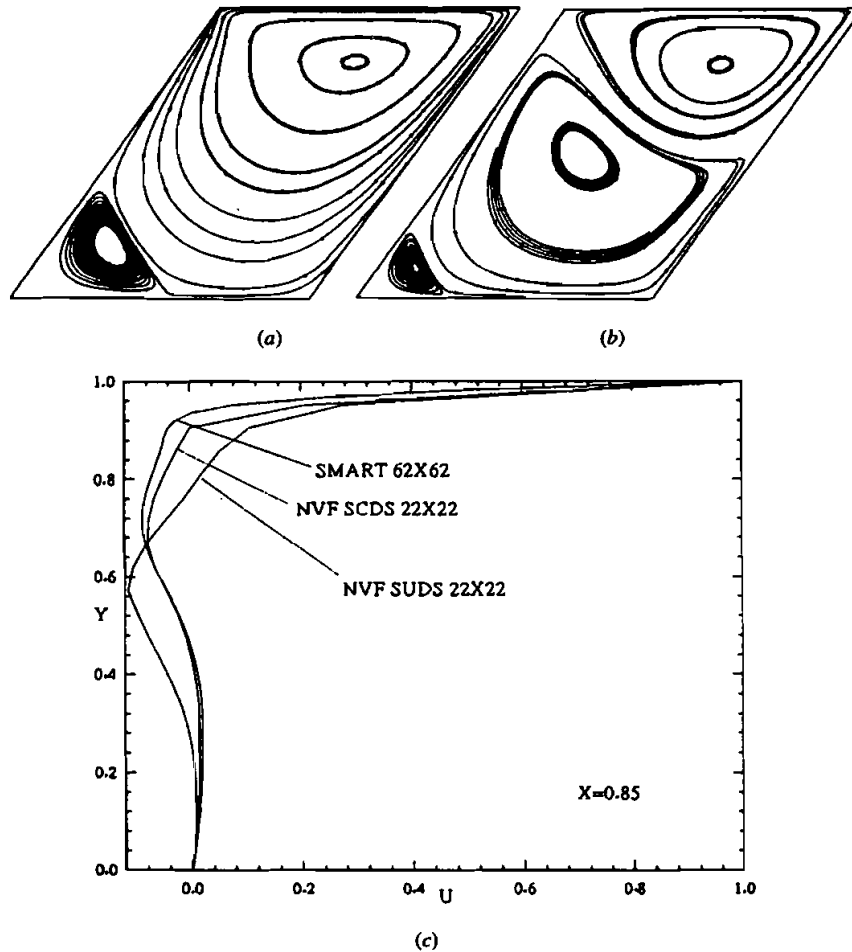
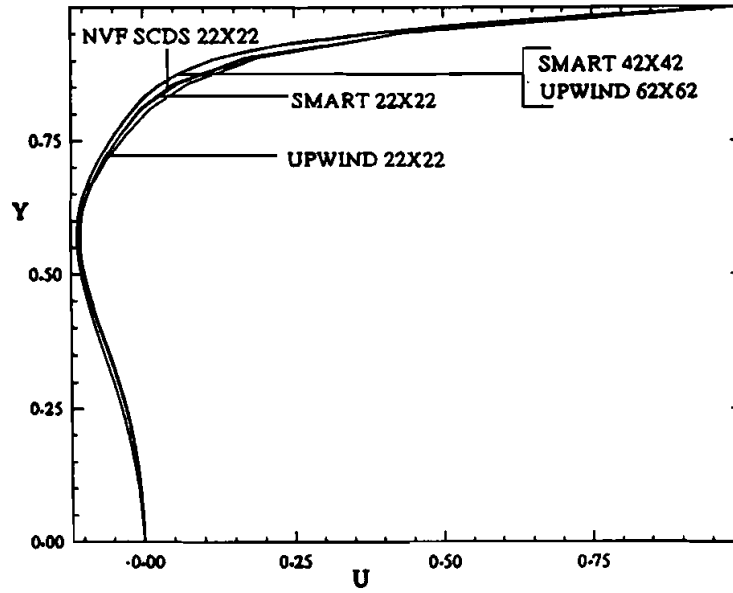
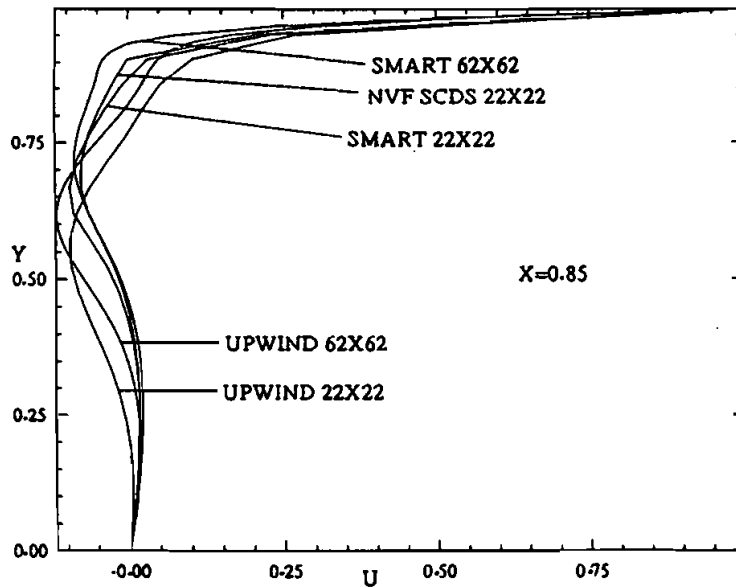


**Figure 5.** Streamlines for driven flow in a skew cavity: (a)  $Re = 100$ ; (b)  $Re = 500$ . (c) Comparison of  $U$ -velocity profiles at  $X = 0.85$  for driven flow in a skew cavity using NVF SCDS, NVF SUDS, and SMART at  $Re = 500$ .

result is even better than the profile obtained by the upwind scheme when using a much denser grid of size  $62 \times 62$ . This outstanding performance of the NVF SCDS is due to its ability to handle both sources of numerical errors arising from the flow skewness and from the important variations in the pressure source term. While the performance of SMART is not greatly affected by the variations of the source because of its high-order interpolation profile, the skewness of the flow degrades its accuracy to a certain degree when the number of grid points is relatively low. The high diffusivity of the upwind scheme is obviously due to its inability to deal with both sources of errors. In conclusion, the previous test problems have clearly demonstrated that for a scheme to be highly accurate, it should be streamline-based and of high-order interpolation profile.



(a)



(b)

Figure 6.  $U$ -velocity profiles at  $X = 0.85$  for a driven flow in a skew cavity using various schemes and grid densities: (a)  $Re = 100$ ; (b)  $Re = 500$ .

#### Test 4: Gradual Expansion in an Axisymmetric, Nonorthogonal Channel

The last problem presented deals with a gradual expansion of a fluid in a nonorthogonal, axisymmetric geometry. A schematic of the physical situation, the computed flow field, the channel's dimensions, and the equation used to generate the channel's surface are depicted in Figure 7. The conservation of mass and momentum equations governing the flow field are given by

$$\frac{\partial U}{\partial X} + \frac{1}{R} \frac{\partial}{\partial R}(RV) = 0 \quad (31)$$

$$\frac{\partial}{\partial X}(U^2) + \frac{1}{R} \frac{\partial}{\partial R}(RUV) = -\frac{\partial P}{\partial X} + \frac{1}{\text{Re}} \frac{\partial}{\partial X} \left( \frac{\partial U}{\partial X} \right) + \frac{1}{\text{Re}} \frac{1}{R} \frac{\partial}{\partial R} \left( R \frac{\partial U}{\partial R} \right) \quad (32)$$

$$\begin{aligned} \frac{\partial}{\partial X}(UV) + \frac{1}{R} \frac{\partial}{\partial R}(RV^2) = & -\frac{\partial P}{\partial R} + \frac{1}{\text{Re}} \frac{\partial}{\partial X} \left( \frac{\partial V}{\partial X} \right) + \frac{1}{\text{Re}} \frac{1}{R} \frac{\partial}{\partial R} \left( R \frac{\partial V}{\partial R} \right) \\ & - \frac{1}{\text{Re}} \frac{V}{R^2} \end{aligned} \quad (33)$$

where the following dimensionless variables have been used:

$$U = \frac{u}{u_{in}} \quad V = \frac{v}{u_{in}} \quad R = \frac{r}{r_i} \quad X = \frac{x}{r_i} \quad P = \frac{p}{\rho u_{in}^2} \quad (34)$$

The boundary conditions employed are

$$U = 1 \quad V = 0 \quad \text{at the inlet} \quad (35)$$

$$U = V = 0 \quad \text{along walls} \quad (36)$$

$$\frac{\partial U}{\partial X} = \frac{\partial V}{\partial X} = 0 \quad \text{at the exit} \quad (37)$$

The problem is solved for a Reynolds number ( $\text{Re} = \rho u_{in} r_i / \mu$ , where  $r_i = 1$ ) of 100. The length  $L$  of the pipe ( $= \text{Re}/3$ ) is long enough to apply the outflow boundary condition safely. The  $U$ -velocity profiles at  $X = 5$  and  $X = 20$ , generated

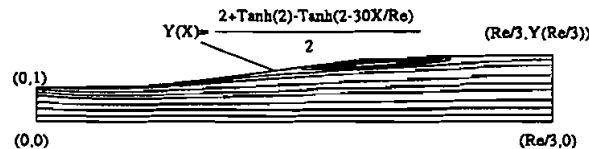
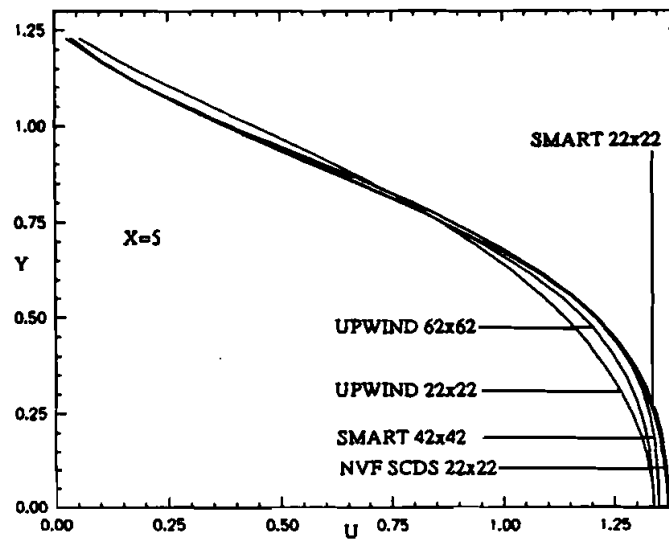
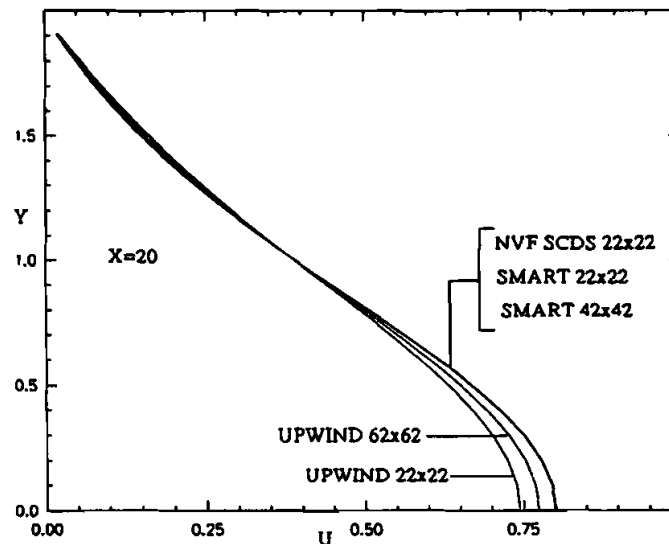


Figure 7. Physical domain and streamlines for gradual expansion in a nonorthogonal, axisymmetric geometry.

using the various schemes and grid densities, are displayed in Figures 8a and 8b, respectively. As shown, the performance of NVF SCDS (a multidimensional second-order scheme) is comparable (slightly better) to that of SMART (a one-dimensional third-order scheme). Both schemes perform, with  $22 \times 22$  grid points, better than the upwind scheme when using  $62 \times 62$  grid points. This slight



(a)



(b)

Figure 8.  $U$ -velocity profiles for gradual expansion in a nonorthogonal, axisymmetric geometry using various schemes and grid densities: (a)  $X = 5$ ; (b)  $X = 20$ .

difference in results between SMART and NVF SCDS is due to the unimportance of cross-stream diffusion and the alignment, more or less, of the flow with the grid lines. This behavior is anticipated, and the problem is deliberately chosen to demonstrate clearly that when streamwise diffusion is dominant and the skewness of the flow with respect to the grid lines is low, the third-order SMART scheme should perform better than the second-order skew scheme (NVF SCDS).

### CONCLUDING REMARKS

A new, bounded, skew central difference scheme was presented. The newly developed high-resolution convective scheme was formulated by combining the skew central difference scheme with the NVF bounding technique. By comparing the performance of the new scheme against the upwind scheme, the NVF SUDS, and the third-order SMART scheme, it can be safely stated that the best performance can always be obtained with high-order skew schemes. For recirculating flow problems (tests 2 and 3), the performance of the second-order skew scheme is much better than that of the SMART scheme. This conclusion will be exploited in a companion article [28] to study natural-convection heat transfer in an eccentric annulus. Therefore, the development of higher-order skew schemes is highly desirable. One issue that should be investigated further is the implementation of such schemes in three-dimensional spaces.

### REFERENCES

1. M. A. Leschziner, Practical Evaluation of Three Finite Difference Schemes for the Computation of Steady-State Recirculating Flows, *Comput. Meth. Appl. Mech. Eng.*, vol. 23, pp. 293–311, 1980.
2. S. V. Patankar, *Numerical Heat Transfer and Fluid Flow*, Hemisphere, New York, 1981.
3. G. D. Raithby, A Critical Evaluation of Upstream Differencing Applied to Problems Involving Fluid Flow, *Comput. Meth. Appl. Mech. Eng.*, vol. 9, pp. 75–103, 1976.
4. A. K. Runchal, Condiff: A Modified Central-Difference Scheme for Convective Flows, *Int. J. Numer. Meth. Eng.*, vol. 24, pp. 1593–1608, 1987.
5. B. P. Leonard, A Survey of Finite Differences with Upwinding for Numerical Modelling of the Incompressible Convective Diffusion Equation, in C. Taylor and K. Morgan (eds.), *Computational Techniques in Transient and Turbulent Flow, Vol. 2*, Pineridge Press, UK, 1981.
6. B. P. Leonard, A Stable and Accurate Convective Modelling Procedure Based on Quadratic Interpolation, *Comput. Meth. Appl. Mech. Eng.*, vol. 19, pp. 59–98, 1979.
7. R. K. Agarwal, A Third Order Accurate Upwind Scheme for Navier Stokes Solutions in Three Dimensions, in K. N. Ghia, T. J. Mueller, and B. R. Patel (Eds.), *Computers in Flow Prediction and Fluid Dynamics Experiments*, ASME Winter Meeting, Washington, DC, pp. 73–82, 1981.
8. J. E. Fromm, A Method for Reducing Dispersion in Convective Difference Schemes, *J. Comput. Phys.*, vol. 3, pp. 176–189, 1968.
9. G. D. Raithby, Skew Upstream Differencing Schemes for Problems Involving Fluid Flow, *Comput. Meth. Appl. Mech. Eng.*, vol. 9, pp. 153–164, 1976.
10. J. N. Lilington, A Vector Upstream Differencing Scheme for Problems in Fluid Flow Involving Significant Source Terms in Steady-State Linear Systems, *Int. J. Numer. Meth. Fluids*, vol. 1, pp. 3–16, 1981.

11. M. A. R. Sharif, An Evaluation of the Bounded Directional Transportive Upwind Differencing Scheme for Convection-Diffusion Problems, *Numer. Heat Transfer*, vol. 23, pp. 201–219, 1993.
12. Y. A. Hassan, J. G. Rice, and J. H. Kin, A Stable Mass-Flow-Weighted Two-Dimensional Skew Upwind Scheme, *Numer. Heat Transfer*, vol. 6, pp. 395–408, 1983.
13. S. T. Zalesak, Fully Multidimensional Flux-Corrected Transport Algorithms for Fluids, *J. Comput. Phys.*, vol. 31, pp. 335–362, 1979.
14. M. Chapman, FRAM Nonlinear Damping Algorithm for the Continuity Equation, *J. Comput. Phys.*, vol. 44, pp. 84–103, 1981.
15. M. Peric, A Finite Volume Method for the Prediction of Three Dimensional Fluid Flow in Complex Ducts, Ph.D. thesis, Imperial College, London, 1985.
16. J. Zhu and M. A. Leschziner, A Local Oscillation-Damping Algorithm for Higher Order Convection Schemes, *Comput. Meth. Appl. Mech. Eng.*, vol. 67, pp. 355–366, 1988.
17. P. K. Sweby, High Resolution Schemes Using Flux Limiters for Hyperbolic Conservation Laws, *SIAM J. Numer. Anal.*, vol. 21, pp. 995–1011, 1984.
18. B. P. Leonard, Simple High-Accuracy Resolution Program for Convective Modelling of Discontinuities, *Int. J. Numer. Meth. Eng.*, vol. 8, pp. 1291–1318, 1988.
19. B. Van Leer, Towards the Ultimate Conservative Difference Scheme. V. A Second-Order Sequel to Godunov's Method, *J. Comput. Phys.*, vol. 23, pp. 101–136, 1977.
20. B. Van Leer, Towards the Ultimate Conservative Difference Scheme. II. Monotonicity and Conservation Combined in a Second Order Scheme, *J. Comput. Phys.*, vol. 14, pp. 361–370, 1974.
21. S. R. Chakravarthy and S. Osher, High Resolution Applications of the OSHER Upwind Scheme for the Euler Equations, AIAA Paper 83-1943, 1983.
22. M. A. R. Sharif and A. A. Busnaina, Evaluation and Comparison of Bounding Techniques for Convection-Diffusion Problems, *J. Fluid Eng.*, vol. 115, pp. 33–40, 1993.
23. J. P. Boris and D. L. Book, Flux-Corrected Transport. I. SHASTA, A Fluid Transport Algorithm That Works, *J. Comput. Phys.*, vol. 11, pp. 38–69, 1973.
24. M. Darwish and F. Moukalled, A New Approach for Building Skew-Upwind Schemes, *Comput. Meth. Appl. Mech. Eng.*, in press.
25. S. G. Rubin and P. K. Khosla, Polynomial Interpolation Method for Viscous Flow Calculations, *J. Comput. Phys.*, vol. 27, pp. 153–168, 1982.
26. P. H. Gaskell and A. K. C. Lau, Curvature Compensated Convective Transport: SMART, A New Boundedness Preserving Transport Algorithm, *Int. J. Numer. Meth. Fluids*, vol. 8, pp. 617–641, 1988.
27. M. Peric, Analysis of Pressure Velocity Coupling on Non-staggered Grids, *Numer. Heat Transfer, Part B*, vol. 17, pp. 63–82, 1990.
28. F. Moukalled and M. Darwish, New Bounded Skew Central Difference Scheme, Part II: Application to Natural Convection in an Eccentric Annulus, *Numer. Heat Transfer, Part B*, vol. 31, pp. 111–133, 1997.
29. M. J. Cho and M. K. Chung, New Treatment of Nonorthogonal Terms in the Pressure-Correction Equation, *Numer. Heat Transfer, Part B*, vol. 26, pp. 133–145, 1994.
30. W. J. Gordon and L. C. Thiel, Transfinite Mappings and Their Applications to Grid Generation, in J. F. Thompson (ed.), *Numerical Grid Generation*, pp. 171–192, North Holland, New York, 1982.